Mon. Not. R. Astron. Soc. **336,** 409–424 (2002)

The effect of non-gravitational gas heating in groups and clusters of galaxies

S. Borgani,[1⋆] F. Governato,[2,7⋆] J. Wadsley,[3⋆] N. Menci,[4⋆] P. Tozzi,[5⋆] T. Quinn,[2⋆] J. Stadel[6⋆] and G. Lake[2⋆]

[1]*INFN, Sezione di Trieste, c/o Dipartimento di Astronomia dell'Università, via Tiepolo 11, I-34131 Trieste, Italy*
[2]*Astronomy Department, University of Washington, Seattle, WA 98195, USA*
[3]*Department of Physics and Astronomy, McMaster University, Hamilton, Ontario, L88 4M1, Canada*
[4]*INAF, Osservatorio Astronomico di Roma, via dell'Osservatorio, I-00040 Monteporzio, Italy*
[5]*INAF, Osservatorio Astronomico di Trieste, via Tiepolo 11, I-34131 Trieste, Italy*
[6]*University of Victoria, Department of Physics and Astronomy, 3800 Finnerty Road, Elliot Building, Victoria, BC V8W 3PG, Canada*
[7]*INAF, Osservatorio Astronomico di Brera, via Brera 28, I-20131 Milano, Italy*

Accepted 2002 June 5. Received 2002 May 16; in original form 2002 March 15

ABSTRACT

We present a detailed study of a set of gas-dynamical simulations of galaxy groups and clusters in a flat, Λ-cold dark matter (ΛCDM) model with $\Omega_{\rm m} = 0.3$, aimed at exploring the effect of non-gravitational heating on the observable properties of the intracluster medium (ICM). We use GASOLINE, a version of the code PKDGRAV that includes a smoothed particle hydrodynamics description of hydrodynamics to simulate the formation of four haloes with virial temperatures in the range $0.5 \lesssim T \lesssim 8$ keV. These simulations resolve the structure and properties of the ICM down to a small fraction of the virial radius, $R_{\rm vir}$. At our resolution X-ray luminosities, $L_{\rm X}$, of runs with gravitational heating only are in good agreement with analytical predictions, which assume a universal profile for CDM haloes, over almost two orders of magnitude in mass.

For each simulated structure, non-gravitational heating of the ICM is implemented in two different ways: (i) by imposing a minimum-entropy floor, $S_{\rm fl}$, at a given redshift, which we take in the range $1 \leqslant z \leqslant 5$; (ii) by gradually heating gas within collapsed regions, proportionally to the supernova rate expected from semi-analytical modelling of galaxy formation in haloes having mass equal to that of the simulated systems.

Our main results are the following. (i) An extra heating energy $E_{\rm h} \gtrsim 1$ keV per gas particle within $R_{\rm vir}$ at $z = 0$ is required to reproduce the observed $L_{\rm X}$–T relation, independent of whether it is provided in an impulsive way to create an entropy floor $S_{\rm fl} = 50$–100 keV cm^2, or is modulated in redshift according to the star formation rate; our supernova (SN) feedback recipe provides at most $E_{\rm h} \simeq 1/3$ keV particle^{-1} and, therefore, its effect on the $L_{\rm X}$–T relation is too small to account for the observed $L_{\rm X}$–T relation. (ii) The required heating implies, in small groups with $T \sim 0.5$ keV, a baryon fraction as low as $\lesssim$40 per cent of the cosmic value at $R_{\rm vir}/2$; this fraction increases to about 80 per cent for a $T \simeq 3$ keV cluster. (iii) Temperature profiles are almost scale-free across the whole explored mass range, with T decreasing by a factor of 3 at the virial radius. (iv) The mass–temperature relation is almost unaffected by non-gravitational heating and follows quite closely the $M \propto T^{3/2}$ scaling; however, when compared with data on the M_{500}–$T_{\rm ew}$ relation, it has a $\sim$40 per cent higher normalization. This discrepancy is independent of the heating scheme adopted. The inclusion of cooling in a run of a small group steepens the central profile of the potential well while removing gas from the diffuse phase. This has the effects of increasing $T_{\rm ew}$ by $\sim$30 per cent, possibly reconciling the simulated and the observed M_{500}–$T_{\rm ew}$ relations, and of decreasing $L_{\rm X}$ by $\sim$40 per cent. However, in spite of the inclusion of SN feedback energy,

⋆E-mail: borgani@ts.astro.it (SB); fabio@hermes.astro.washington.edu (FG); trq@hermes.astro.washington.edu (TQ); lake@hermes.astro.washington.edu (GL); wadsley@physics.mcmaster.ca (JW); menci@coma.mporzio.astro.it (NM); tozzi@ts.astro.it (PT); stadel@phys.uvic.ca (JS)

almost 40 per cent of the gas drops out from the hot diffuse phase, in excess of current observational estimates of the number of cold baryons in galaxy systems.

It is likely that only a combination of different heating sources (SNe and active galactic nuclei) and cooling will be able to reproduce both the $L_{\rm X}$–$T_{\rm ew}$ and M_{500}–$T_{\rm ew}$ relations, as observed in groups and clusters, while balancing the cooling runaway.

Key words: hydrodynamics – galaxies: clusters: general – cosmology: miscellaneous – X-rays: galaxies.

1 INTRODUCTION

The X-ray emission from clusters of galaxies offers a unique means of studying the physics of cosmic baryons and their connection with the processes of galaxy formation and evolution. The first attempt to model the intracluster medium (ICM) within the framework of the hierarchical clustering scenario, assumed its thermodynamical properties to be entirely determined by gravitational processes, such as adiabatic compression during collapse and shock heating by supersonic gas accretion (Kaiser 1986). Since gravity does not have characteristic scales, for an Einstein–de Sitter cosmology this model predicts rich massive clusters and poor groups to appear as scaled versions of each other. Under the assumptions of emissivity dominated by free–free bremsstrahlung and of hydrostatic equilibrium of the gas, this model predicts $L_{\rm X} \propto T^2(1+z)^{3/2}$ for the shape and evolution of the relation between X-ray luminosity and gas temperature. Furthermore, if we define the gas entropy as $S = T/n_{\rm e}^{2/3}$ (where $n_{\rm e}$ is the electron number density; e.g. Eke, Navarro & Frenk 1998), then the self-similar ICM has $S \propto T(1+z)^{-2}$.

This simple model was quickly recognized to fail to account for several observational facts: (a) the $L_{\rm X}$–T relation for nearby clusters is steeper than predicted, with $L_{\rm X} \propto T^{\sim 3}$ for $T \gtrsim 2$ keV clusters (e.g. David et al. 1993; White, Jones & Forman 1997; Allen & Fabian 1998; Markevitch 1998; Arnaud & Evrard 1999), with a possible further steepening at the group scale, $T \lesssim 1$ keV (Ponman et al. 1996; Helsdon & Ponman 2000); (b) no evidence of evolution for its amplitude has been detected out to $z \gtrsim 1$ (e.g. Mushotzky & Scharf 1997; Donahue et al. 1999; Fairley et al. 2000; Della Ceca et al. 2000; Borgani et al. 2001b; Holden et al. 2002); (c) the gas density profile in central regions of cooler groups is relatively softer than in clusters and, correspondingly, the entropy is higher than predicted by self-similar scaling (e.g. Ponman, Cannon & Navarro 1999; Lloyd-Davies, Ponman & Cannon 2000; Finoguenov et al. 2002); (d) colder clusters contain a relatively smaller amount of gas than very hot ones (e.g. Neumann & Arnaud 2001).

A common interpretation for such observational facts requires non-gravitational energy input, which should have taken place during the past history of the ICM. This extra heating would place the gas on a higher adiabat and sustain the gas during the gravitational collapse of the cluster dark matter (DM) halo, preventing it from reaching a high density in central regions and suppressing the X-ray emission. For a fixed specific amount of heating energy per gas particle, the effect is larger for the smaller systems, while it is negligible for more massive, hotter systems. Kaiser (1991) suggested for the first time that gas pre-heating and subsequent adiabatic collapse turns into a differential steepening of the $L_{\rm X}$–T relation at the cluster scales. Evrard & Henry (1991), Navarro, Frenk & White (1995) and Bower (1997) assumed the gas in the cluster core to have a minimum-entropy level, which was established at some pre-heating epoch.

Although this model produces an $L_{\rm X}$–T relation steeper than the self-similar prediction, it fails to account for the further steepening at the group scale (Ponman et al. 1996). Cavaliere, Menci & Tozzi (1998, 1999) were able to predict the correct $L_{\rm X}$–T slope, both at the cluster and at the group scale, by assuming a pre-heated gas at a temperature $T \sim 0.5$ keV, which is shocked with different strengths when falling into groups and clusters. A pre-heating producing an isentropic gas distribution has been assumed by Balogh, Babul & Patton (1999), Tozzi & Norman (2001, TN01 hereafter) and Babul et al. (2002). In particular, TN01 worked out a series of predictions of observables properties of the ICM with isentropic pre-heating, including the amount of energy feedback required to produce the correct $L_{\rm X}$–T relation and entropy threshold at the group scale. Brighenti & Mathews (2001) discussed the effect of heating the gas either when it has still to collapse within clusters and groups (external heating) or when it is already accreted (internal heating). They concluded that internal heating is more efficient at accounting at the same time for both the slope of the $L_{\rm X}$–T relation and the excess entropy in poor clusters.

While most such analyses agree that an extra heating energy of $\sim$0.5–1 keV per gas particle is required, no general consensus has yet been reached concerning its astrophysical origin. Supernovae (SNe) have been advocated by several authors as a possible source for pre-heating (e.g. Wu, Fabian & Nulsen 1998) and metal enriching (e.g. Loewenstein & Mushotzky 1996; Renzini 1997; Finoguenov & Ponman 1999; Pipino et al. 2002) the ICM. Although some analyses showed that SNe can actually provide an adequate energy budget (Menci & Cavaliere 2000; Lloyd-Davies et al. 2000), other authors claimed that this requires a very high, possibly unrealistic, efficiency for the thermalization of the released energy (Wu, Fabian & Nulsen 2000; Kravtsov & Yepes 2000; Bower et al. 2001).

In this case, alternative sources for ICM heating are required, such as SNe from a primordial star population, the so-called Population III stars (e.g. Loewenstein 2001), and nuclear galactic activity associated with quasi-stellar objects (QSOs) (e.g. Valageas & Silk 1999; McNamara et al. 2000; Yamada & Fujita 2001; Nath & Roychowdhury 2002). As for Population III stars, one expects them not to significantly heat the diffuse medium, in order not to destroy Ly-α absorbers at lower redshift, $z \lesssim 3$, and not to overpollute the IGM with metals.

To date, only a few attempts have been pursued to address in detail the effects of non-gravitational heating on X-ray observable quantities with numerical hydrodynamical simulations (Navarro et al. 1995; Pen 1999; Lewis et al. 2000; Borgani et al. 2001a; Valdarnini 2002). Bialek, Evrard & Mohr (2001) have realized a large set of moderate resolution simulations of clusters and groups, setting different entropy floors at very high redshift. They found that agreement with observational constraints on X-ray cluster scaling properties requires an entropy floor of about 100 keV cm^2, which, at their heating redshift $z_{\rm h} \simeq 21$, corresponds to an extra energy of about 0.2 keV particle^{-1}.

As an alternative to extra heating, radiative cooling has also been suggested as a mechanism to break ICM self-similarity. In this case, X-ray luminosity is suppressed as a consequence of the reduced amount of gas in the hot diffuse phase (Pearce et al. 2000; Muanwong et al. 2001). In addition, low-entropy gas in central cluster regions is selectively removed from the hot phase as a consequence of its short cooling time, thus leaving only high entropy gas (Voit & Bryan 2001). However, cooling in itself is known to convert into a cold stellar phase a large fraction of gas, >30 per cent (e.g. Lewis et al. 2000; Davé et al. 2001), much larger than the $\lesssim$10 per cent baryon fraction locked into stars indicated by observations. This underlines the need for extra heating to prevent overcooling of the ICM (e.g. Suginohara & Ostriker 1998; Prunet & Blanchard 1999; Balogh et al. 2001).

The main aim of this paper is to study in detail the effect of non-gravitational energy injection into the ICM and how much of this energy is needed to correctly reproduce different X-ray observable properties of groups and clusters of galaxies. In a previous paper (Borgani et al. 2001a, Paper I hereafter) we concentrated on the effect of non-gravitational heating on the entropy pattern of the ICM. As a main conclusion, we showed that the entropy excess in the central regions of poor clusters (Ponman et al. 1999) requires an extra heating of about 1 keV particle^{-1}. This paper presents an extended analysis of a larger set of simulations, which include several schemes of ICM extra heating. We will also show results from a simulation of a poor group, which includes gas cooling and a star formation algorithm to remove dense cold gas particles from the smoothed particle hydrodynamics (SPH) computation. This simulation will be used to discuss the role that cooling plays in determining the ICM thermodynamics.

The plan of the paper is as follows. In Section 2 we give a short description of the Tree+SPH code GASOLINE and provide details concerning the simulations. Section 3 describes the different recipes for non-gravitational heating that we used. Section 4 is devoted to the presentation of the results. In Section 5 we discuss the effect of cooling, while a summary of our main results and our conclusions are presented in Section 6.

2 NUMERICAL METHOD

2.1 The code

We use GASOLINE, a new *N*-body/smoothed particle hydrodynamics code. GASOLINE performs gravity and hydrodynamics operations using a binary tree structure with periodic boundary conditions for cosmology. It uses concurrent multiple time-steps for increased throughput and runs in parallel on a wide variety of architectures using, e.g. pthreads, shared memory or the Message Passing Interface (MPI). The code handles gravity, pressure gradients, hydrodynamic shocks, radiative cooling, photoionizing ultraviolet (UV) background and was extended for this work to incorporate external heating sources. For a full description of GASOLINE, including extended tests of the code, see Wadsley, StadGel & Quinn (in preparation). For a description of the gravity code on which GASOLINE is based, see Stadel (2001). The external heating SN described in Section 3 is treated within the code as an additional component added locally to the standard SPH compressive heating ('$P\,\mathrm{d}V$') term.

As a demonstration of the effectiveness of GASOLINE for cluster simulations, we evolve the initial conditions from the 'Santa Barbara Cluster Comparison' (Frenk et al. 2000). We resolve the resulting luminous X-ray cluster with ∼15 000 gas particles within the virial radius (2.7 Mpc) at the current epoch with 64^3 gas and 64^3 dark matter particles in the whole box. This resolution was used by the majority of the cluster comparison SPH codes including the widely used HYDRA code (Couchman 1991). The test evolved the gas adiabatically without additional heat sources or sinks. The gas profiles for GASOLINE with curves for HYDRA and the average result from the cluster comparison are shown in Fig. 1. The innermost radial bin plotted in each case is indicative of the resolution. The variation seen is similar to that found between cluster comparison code results, even among different SPH codes, caused by differing implementations and the interpretation of the initial condition data that were given to the coders at 256^3 resolution. The central temperature is sensitive, in particular, to shock treatment and, most of all, minor variations in the timing of small subclump mergers (for an extended

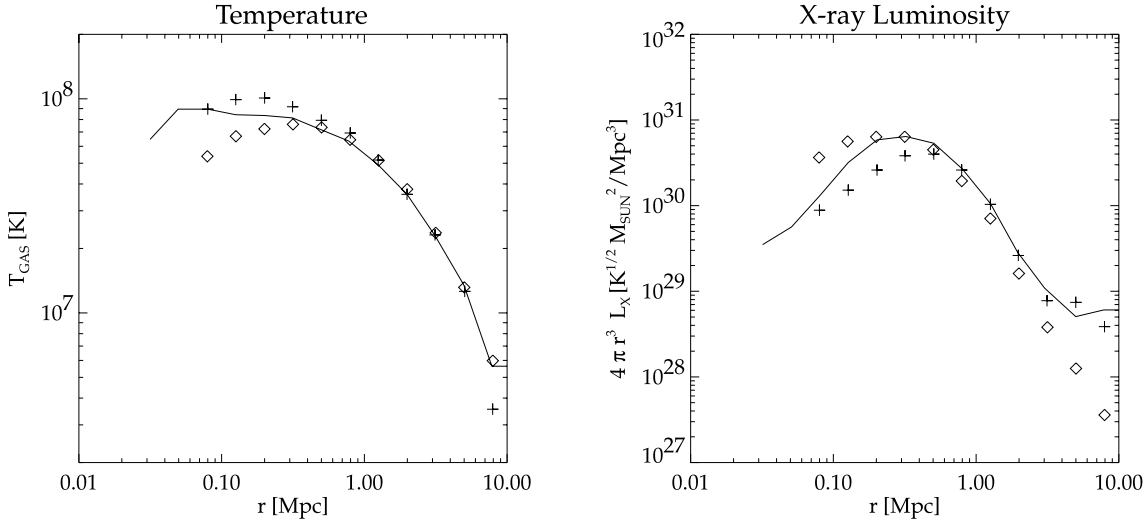

Figure 1. 'Cluster comparison' gas profiles. The GASOLINE results at 64^3 (diamonds) for the temperature (left) and X-ray luminosity (right) profiles are in excellent agreement with the averaged results from different codes (solid line) and HYDRA (plus symbols) profiles from the cluster comparison paper (Frenk et al. 2000).

discussion see Wadsley et al. 2002, in preparation). Except for these small variations, the GASOLINE results are in excellent agreement with the other codes.

2.2 The simulations

We simulated at high resolution four haloes taken from a DM-only cosmological simulation within a 100-Mpc box of a Λ-cold dark matter (ΛCDM) model with $\Omega_m = 0.3, \Omega_\Lambda = 0.7, \sigma_8 = 1$ and Hubble constant $H_0 = 70\ \mathrm{km\ s^{-1}\ Mpc^{-1}}$. The baryon density parameter was chosen to be $\Omega_\mathrm{b} = 0.019\ h^{-2}$, as inferred from the high deuterium abundance detected in QSO absorption lines (e.g. Burles & Tytler 1998), which corresponds to a baryon fraction $f_\mathrm{bar} \simeq 0.13$.

From the simulated box we selected four haloes with masses corresponding to virial temperatures in the range $0.5 \lesssim T \lesssim 8$ keV. With this choice, we are sure to encompass the temperature interval where the L_X–T relation is observed to steepen substantially and where the effect of energy injection should be more important. The sizes of the four simulated structures are of the same order as those of the Coma cluster (e.g. Geller, Diaferio & Kurtz 1999), the Virgo cluster (Bingelli, Tammann & Sandage 1987), the Fornax group (e.g. Drinkwater et al. 2000) and of a smaller Hickson-like group (e.g. Pildis, Bregman & Evrard 1995). In the following we indicate with these names the corresponding simulated structures.

Using the so-called renormalization technique (Katz & White 1993), the simulation within the periodic box is centred around each resimulated halo, the mass distribution and the perturbation spectrum are resampled at higher resolution within the Lagrangian region that contains the halo of interest. The high-resolution region extends typically for a few comoving Mpc around the halo. The outer regions are resampled at decreasing resolution. As the four haloes span almost two decades in mass, the numerical resolutions differ accordingly, so as to keep comparable the number of particles within the virial radius and the force resolution in units of the virial radius. Typically, 0.5–1.5 $\times\ 10^6$ particles are used for each run, with about half of them used to simulate the high-resolution central regions. A summary of the characteristics of the simulations are reported in Table 1. Note that halo particle number refers to the number of particles within the virial radius, and not just in the high-resolution region, which typically contains a few times more particles. In order to investigate the effect of resolution, the Virgo, Fornax and Hickson runs have been realized with different mass and force resolution. The high-resolution version of each run has a force softening, which is at most 1 per cent of the virial radius, while the mass resolution is chosen so that at least 5×10^4 gas particles fall within that radius by $z = 0$. For all the runs we used $\eta = 0.2$ and a force accuracy parameter of the tree algorithm of $\theta = 0.7$ ($\theta = 0.5$ for $z > 2$), as suggested by Moore et al. (1998) and later verified by Power et al. (2002), for the parameters regulating time accuracy of the integration and the accuracy of the tree algorithm.

We show in Fig. 2 the gas density maps for the high-resolution regions of the simulated structures at $z = 0$. The quite high resolution achieved allows us to resolve numerous substructures. Some of them retain part of their individual gas content, which survives for a few crossing times before being stripped, as well as discontinuities associated with bow shocks (see Paper I for a discussion of these features as seen from the entropy maps of simulations). It is tempting to associate such structures to the small-scale features revealed by *Chandra* observations, which in some cases are associated with bow shocks or cold fronts from merging structures (e.g. Markevitch et al. 2000; Mazzotta et al. 2001; Ettori & Fabian 2001, and references therein). At $z = 0$ the Coma-like halo is undergoing several merging events with massive subgroups, at different stages of advancement, much like what is seen in the *XMM* observations of the real Coma cluster (Briel et al. 2001).

Table 1. Characteristics of the simulated haloes and numerical parameters of the simulations. Column 2, simulation version (HR, high resolution; LR, low resolution); column 3, total mass within the virial radius at $z = 0$($10^{13}\ \mathrm{M_\odot}$); column 4, virial radius (Mpc); column 5, mass of gas particles ($10^8\ \mathrm{M_\odot}$); column 6, mass of DM particles within the resimulated region ($10^8\ \mathrm{M_\odot}$); columns 7 and 8, number of gas and DM particles within the virial radius; column 9, softening parameter (kpc; runs marked with $*$ have been run also with a twice as large softening); column 10, starting redshift.

Run		M_vir	R_vir	m_gas	m_DM	N_gas	N_DM	ϵ	z_in
Coma		133.6	2.86	17.7	119.2	0.99e5	0.90e5	7.5	49
Virgo	HR	30.4	1.75	2.21	14.9	1.70e5	1.79e5	7.5	69
	LR			17.7	119.2	0.21e5	0.22e5	15	49
Fornax	HR	5.91	1.01	0.65	4.41	1.06e5	1.18e5	2.5*	89
	LR			5.20	35.3	1.33e4	1.48e4	7.5	69
Hickson	HR	2.49	0.76	0.65	4.41	4.93e4	4.86e4	2.5*	89
	LR			5.20	35.3	0.62e4	0.61e4	7.5	69

2.3 Definitions of observables

The bolometric luminosity for a set of N_gas gas particles is defined as

$$L_\mathrm{X} = \frac{m_\mathrm{gas}}{\mu m_\mathrm{p}} \sum_{i=1}^{N_\mathrm{gas}} \frac{\rho_i}{\mu m_\mathrm{p}} \Lambda_\mathrm{c}(T_i), \tag{1}$$

where m_p is the proton mass, m_gas is the mass of a gas particle (see Table 1), ρ_i and T_i are the density and temperature at the position of the ith particle, respectively, and $\mu = 0.6$ is the mean molecular weight for a primordial gas composition with 76 per cent mass provided by hydrogen. Assuming that the main contribution to the X-ray emission is from free–free bremsstrahlung, the cooling function turns out to be $\Lambda_\mathrm{c}(T) = 1.2 \times 10^{-24} (kT/\mathrm{keV})^{1/2}\ \mathrm{erg\ cm^3\ s^{-1}}$ (e.g. Navarro et al. 1995).

Under the assumption of isothermal gas following the spherically symmetric DM distribution, it can be shown that the bolometric X-ray luminosity is

$$L_\mathrm{X} = \left(\frac{f_\mathrm{gas}}{3\mu m_\mathrm{p}} \right)^2 \Delta_\mathrm{vir} M_\mathrm{vir} \bar{\rho} F(c) \Lambda_\mathrm{c}(T) \tag{2}$$

(e.g. Eke et al. 1998) where f_gas is the gas fraction within the cluster, Δ_vir is the overdensity corresponding to virialization ($\simeq$178 for $\Omega_m = 1$; Eke, Cole & Frenk 1996), $\bar{\rho}$ is the average cosmic density and M_vir is the virial cluster mass (i.e. the mass enclosed within the radius R_vir within which the average density is $\Delta_\mathrm{vir}\bar{\rho}$). Under the above assumptions, mass and temperature are related according to

$$k_\mathrm{B} T = \frac{1.38}{\beta} \left(\frac{M_\mathrm{vir}}{10^{15} h^{-1} \mathrm{M_\odot}} \right)^{2/3} [\Omega_m \Delta_\mathrm{vir}(z)]^{1/3} (1+z)\ \mathrm{keV} \tag{3}$$

(e.g. Eke et al. 1996). The β parameter is defined as the ratio of the specific kinetic energy of the collisionless DM to the specific thermal energy of the gas,

$$\beta = \frac{\mu m_\mathrm{p} \sigma_v^2}{k_\mathrm{B} T}, \tag{4}$$

where σ_v the one-dimensional velocity dispersion of DM particles. For a (Navarro et al. 1997, hereafter NFW) density profile, $F(c)$ is a function of the concentration parameter c only:

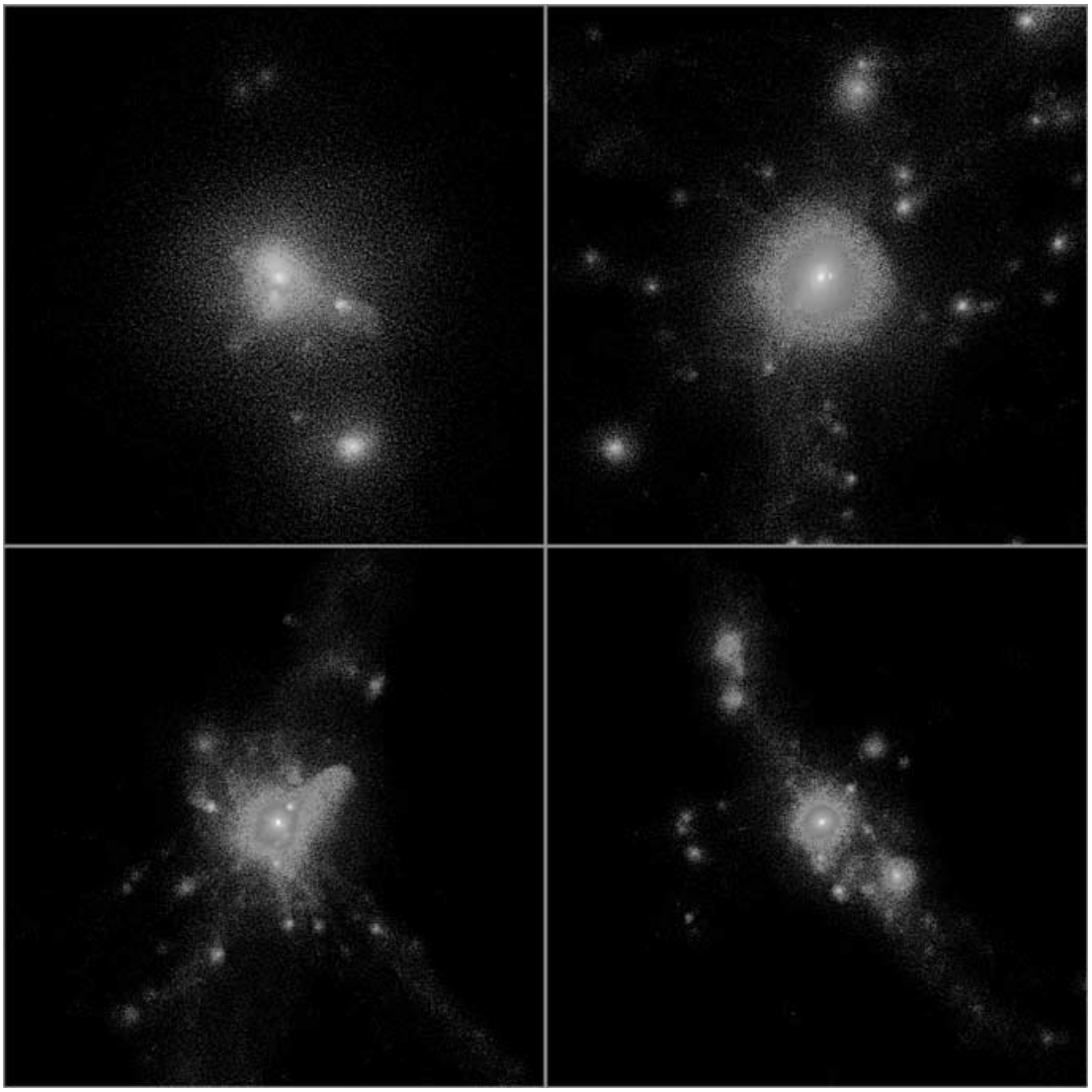

Figure 2. The map of the gas density for the HR version of the four simulated structures. The Coma, Virgo, Fornax and Hickson runs correspond to the upper left, upper right, lower left and lower right-hand panels, respectively. Each box correspond to a physical size of 10 Mpc. This figure can be seen in colour on *Synergy*, in the online version of the journal.

$$F(c) = c^3 \frac{1-(1+c)^{-3}}{[\ln(1+c) - c/(1+c)]^2}. \quad (5)$$

For the sake of comparison between the prediction of equation (2) with the results from simulations, we compute the concentration parameter as a function of the halo mass for our choice of cosmological parameters following the prescription of Eke, Navarro & Steinmetz (2001).

Besides the bremsstrahlung emission, line emission gives a non-negligible contribution at temperatures $T < 2$ keV. To account for it and correctly compare our results with observations, we use the code of Raymond & Smith (1977) in the XSPEC package to estimate the emissivity of a plasma with metallicity $Z = 0.3\,Z_{\odot}$.

We define the mass-weighted temperature of the cluster as

$$T_{\rm mw} = \frac{1}{N_{\rm gas}} \sum_i T_i, \quad (6)$$

where the sum is over all the particles falling within the cluster virial radius. A more useful quantity for comparison with observations is the emission-weighted temperature, which is defined as

$$T_{\rm ew} = \frac{\sum_i \rho_i T_i^{3/2}}{\sum_i \rho_i T_i^{1/2}}. \quad (7)$$

This definition strictly holds only for bremsstrahlung emissivity. We verified that final values of $T_{\rm ew}$ are essentially unchanged if we account for the contribution from metal lines.

Finally, we define the gas entropy carried by the ith particle as

$$s_i = \frac{kT_i}{n_{{\rm e},i}^{2/3}}\,{\rm keV\,cm^2}, \quad (8)$$

where $n_{{\rm e},i}$ is the electron number density associated with that particle.

In Table 2 we give the values of bolometric luminosity, mass and emission-weighted temperatures for the simulated structures and for the different pre-heating schemes (see below).

2.4 Effects of resolution

It is generally regarded that a few thousand DM particles within the virial radius are required to describe global quantities, such as

Table 2. Quantifying the simulated ICM at $z = 0$. Column 1 shows the type of the run and corresponding label. For the runs with SN feedback η represents the fraction of the total energy released by SN which is thermalized into the ICM. For the S-50 and S-100 runs, $S_{\rm fl}$ indicates the value of the entropy floor set at $z = 3$. $L_{\rm br}$ is the X-ray luminosity from bremsstrahlung emission (10^{43} erg s^{-1}); $L_{\rm RS}$ is the X-ray luminosity using a Raymond–Smith code to account for the contribution from line emission, assuming $Z = 0.3\,{\rm Z}_\odot$ for the average gas metallicity 10^{43} erg s^{-1}); $T_{\rm mw}$ and $T_{\rm ew}$ are mass-weighted and emission-weighted temperature within $R_{\rm vir}$ (keV). The asterisks mark the simulations for which only the LR runs are available.

Run type	Coma				Virgo				Fornax				Hickson			
	$L_{\rm br}$	$L_{\rm RS}$	$T_{\rm mw}$	$T_{\rm ew}$	$L_{\rm br}$	$L_{\rm RS}$	$T_{\rm mw}$	$T_{\rm ew}$	$L_{\rm br}$	$L_{\rm RS}$	$T_{\rm mw}$	$T_{\rm ew}$	$L_{\rm br}$	$L_{\rm RS}$	$T_{\rm mw}$	$T_{\rm ew}$
Grav. heating (GH)	139	160	5.1	5.8	35.2	42.0	1.99	2.70	6.52	10.7	0.69	0.95	1.61	3.87	0.39	0.60
SN feedback ($\eta = 0.1$, SN-0.1)													0.73*	1.71*	0.38*	0.60*
SN feedback ($\eta = 1$, SN-1)					32.0	37.7	2.01	2.75	3.63	5.65	0.68	1.02	0.45	1.02	0.39	0.63
SN feedback ($\eta = 4$, SN-4)													1.8e−2	3.8e−2	0.46	0.62
$S_{\rm fl} = 50$ keV cm^2 (S-50)	103	117	5.2	7.2	14.3	16.7	2.07	3.00	0.38	0.67	0.60	0.94	0.04	0.10	0.39	0.58
$S_{\rm fl} = 100$ keV cm^2 (S-100)					3.2	3.8	1.99	2.77	9.9e−2	0.18	0.58	0.90	1.1e−2	2.4e−2	0.40	0.58
Cooling SN-1													3.1e−2	6.1e−2	0.41	0.81

the total virial mass $M_{\rm vir}$ and the velocity dispersion σ_v, and as many gas particles are also sufficient to correctly estimate the ICM temperature. However, a resolution higher by about one order of magnitude is required to correctly describe the X-ray luminosity: since this quantity depends on the square of the local gas density, its correct computation requires the details of cluster structure in the innermost regions and gas clumping to be accurately resolved (e.g. Anninos & Norman 1996; Navarro et al. 1995; Eke et al. 1998; Bryan & Norman 1998; Lewis et al. 2000).

Resolution is even more an issue if one wants to properly resolve the internal structure of the ICM, including shock patterns of the infalling gas, which carry information on the physics of the diffuse medium. The higher the resolution, the larger the number of substructures surviving within the virial radius of the main cluster halo. The largest subhalos are able to keep a fraction of their gas and can carry it down to the centre of the main halo, possibly shocking the gas and raising the central entropy. The X-ray luminosity profiles also depend on the underlying matter profile, for which about 100 000 particles are necessary to avoid underestimating its central density (Moore et al. 1998).

In Fig. 3 we compare the relation between X-ray luminosity and mass-weighted temperature, $T_{\rm mw}$, for the HR and LR runs with gravitational heating (GH) only. Increasing the resolution has a non-negligible effect on the estimated X-ray luminosity, while, as expected, it has only a marginal effect on the mass-weighted temperature. The $L_{\rm X}$ value for the HR run of the Virgo cluster is $\sim$25 per cent higher than for the LR run, the difference increasing to $\sim$50 per cent for the Fornax group and to $\sim$100 per cent for the Hickson group. We have also verified that decreasing the softening by a factor of 2 for the Fornax and Hickson runs, while keeping the mass resolution fixed, increases $L_{\rm X}$ by about 10 per cent, thus showing that the adopted spatial resolution is adequate to resolve all the structures, which are responsible for the X-ray emission. In fact, at the highest resolution of our runs, the number of massive subhalos (i.e. with circular velocity larger than one-tenth of that of the main halo) is likely to have converged (Ghigna et al. 2000). We expect spatial resolution to be even less of an issue when considering simulations with extra heating (see below). Indeed, in this case the gas is put on a higher adiabat and, therefore, does not follow the small-scale potential wells, which are characterized by a virial temperature of a few tens of keV.

We stress that the HR runs predict an $L_{\rm X}$–T relation, which agrees well, both in slope and normalization, with the prediction of the scaling model of equation (2) for a pure bremsstrahlung cooling function. We consider this agreement as a convincing indication that

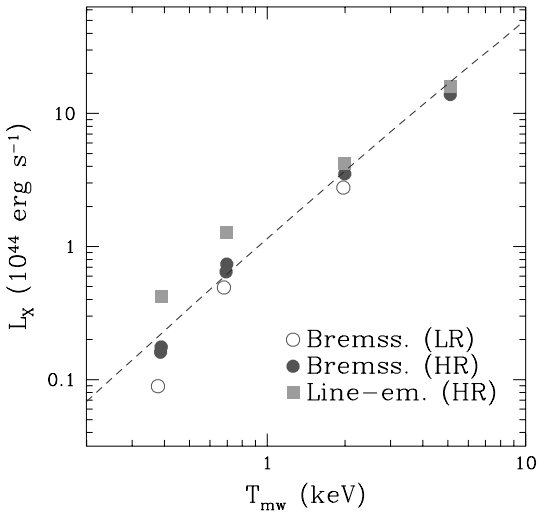

Figure 3. The effect of numerical resolution and line emission on the relation between X-ray luminosity and mass-weighted temperature for the GH runs. Open and solid circles refer to pure bremsstrahlung luminosity for the set of low- and high-resolution runs, respectively (see Table 1). Squares are for luminosity computed by accounting for the contribution from line emission, estimated from a Raymond–Smith code assuming $Z = 0.3\,{\rm Z}_\odot$ for the global ICM metallicity. For the Fornax and Hickson runs, the almost overlapping lower and upper circles are for softening parameter $\epsilon = 5$ and 2.5 kpc, respectively (see text). The dashed line is the prediction of the model described in the text, based on a bremsstrahlung cooling function, an NFW profile for the dark matter halo, with concentration parameter appropriate for the simulated cosmology, and an $M_{\rm vir} - T$ relation given by equation (3) with $\beta = 1$. This figure can be seen in colour on *Synergy*, in the online version of the journal.

the HR runs provide a correct description of the gas distribution, which requires using at least $\simeq 5 \times 10^4$ particles within the virial radius. This result is in agreement with that from resolution studies involving the collisionless component only (e.g. Moore et al. 1998), which established the minimum number of particles required to correctly model the central profile of dark matter haloes. Fig. 3 also highlights a common problem of simulations of large cosmological volumes at *fixed mass resolution*: as the resolution becomes worse for smaller masses, $L_{\rm X}$ becomes underestimated. For instance, taking the same resolution for the Virgo, Fornax and Hickson runs would produce spurious steepening of the $L_{\rm X}$–T relation. Finally, while a pure bremsstrahlung emissivity is a good approximation at

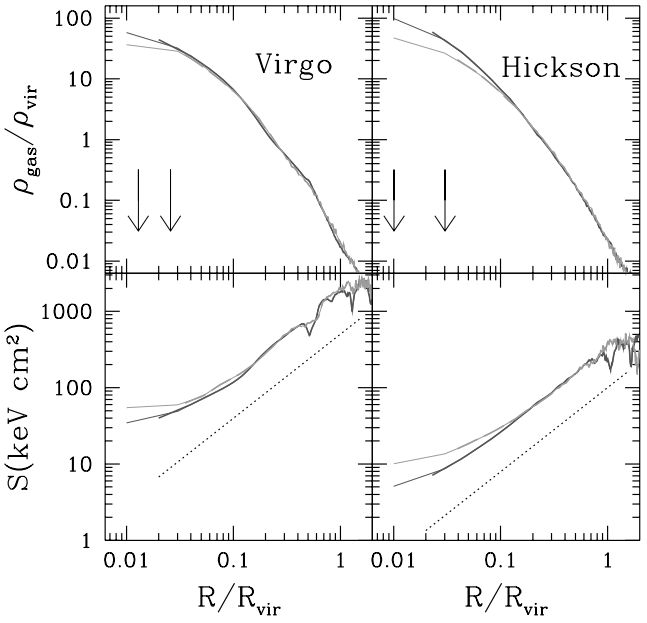

Figure 4. Effect of resolution on the profiles of gas density (upper panels) and specific entropy (lower panels) for the GH version of the Virgo and Hickson simulations. In each panel continuous and dashed curves correspond to the HR and LR runs, respectively. Curves become thinner at the radius containing 100 gas particles. The vertical arrows mark the scale corresponding to three times the value of the Plummer-equivalent force softening for the LR and HR runs (see Table 1), therefore close to the actual spline softening length. The dotted lines in the lower panels show the $S \propto R^{1.1}$ entropy profile predicted by the semi-analytical model by TN01. This figure can be seen in colour on *Synergy*, in the online version of the journal.

$T \gtrsim 2$ keV, the effect of line emission is shown to become important for smaller/cooler systems. The net effect of properly accounting for them is that of flattening the L_X–T relation, thus further increasing the discrepancy with respect to observations at the scale of poor clusters and groups.

In Fig. 4 we show the effect of the resolution on the profiles of gas density and mean entropy per particle. There is an overall good convergence of these quantities, at the radii encompassing at least 100 gas particles (tick curves), with slight deviations at somewhat larger scales for the Hickson run. This number of particles corresponds to about three times the number of neighbours over which the SPH smoothing length is estimated. Therefore, the radius containing this many particles indicates the smallest scale, which is resolved by the SPH kernel with the given softening. On smaller scales the gas density tends to be somewhat underestimated and so is the X-ray luminosity, while two-body heating causes some flattening of the entropy profile (e.g. Steinmetz & White 1997; Yoshida et al. 2001). As the mass and the spatial resolutions are increased, gas and entropy profiles steepen in the innermost regions. The absence of an entropy core agrees with predictions from analytical models based on gravitational gas heating and spherical accretion: gas residing in the central cluster regions has been accreted at the very beginning and, therefore, never significantly shocked, thus preserving its initial low entropy.

Besides extra heating, a further possibility to increase the entropy level in central cluster regions could be by anisotropic accretion of gas, which has been previously gravitationally shocked by large-scale filaments. In order to verify this possibility, we identify at $z = 0$ gas particles in the central region of a halo and trace

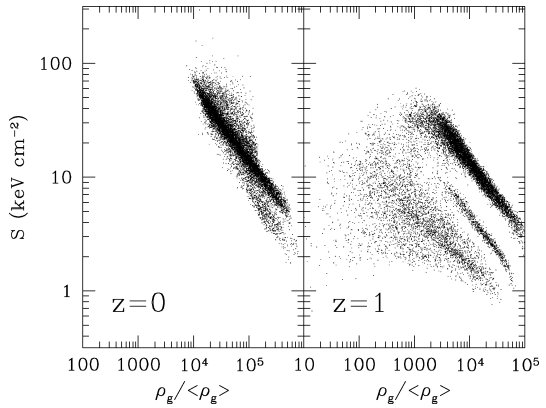

Figure 5. Gas entropy versus overdensity for particles of the Fornax group, which fall within $0.1R_{vir}$ at $z = 0$ (left-hand panel) and traced back to $z = 1$ (right-hand panel).

them back at higher redshift. As an example, we show in Fig. 5 the density–entropy scatter plot for the gas particles falling at $z = 0$ within $0.1R_{vir}$ in the HR Virgo simulation, and their corresponding distribution at $z = 1$. In the left-hand panel these particles define a darker strip, which correspond to the cluster core, while the lighter strip at lower entropy witnesses the presence of a merged subclump, which still preserves its identity (see also Fig. 2). At $z = 1$ these same particles define several individual subclumps, which by the present time have merged together at the centre of the main halo. Such groups at $z = 1$ correspond to lower-entropy structures, in line with the expectation that the gas within smaller structures undergoes weaker shocks. Gas possibly accreted along filaments would correspond at $z = 1$ to structures with density contrast $\delta \sim 10$ containing shocked gas with $S \gtrsim 50$ keV cm^2. Actually, there is no trace of such gas particles in the right-hand panel of Fig. 5. This shows that gas accreted along filaments does not penetrate efficiently into the cluster central region and contribute to increasing the entropy there.

3 BEYOND GRAVITATIONAL HEATING

3.1 Entropy floor

Our first scheme for non-gravitational heating is based on setting a minimum-entropy value at some pre-collapse redshift (e.g. Navarro et al. 1995; Bialek et al. 2001; TN01). For gas with local electron number density n_e and temperature T, expressed in keV, at redshift z, we define the entropy as

$$S = \frac{T}{n_e^{2/3}} = \left[\frac{f_{bar}}{m_p}\frac{1+X}{2}\bar{\rho}(z_h)\,(1+\delta_g)\right]^{-2/3} T \text{ keV cm}^2, \qquad (9)$$

where $\bar{\rho}(z) = \bar{\rho}_0(1+z)^3$ is the average cosmic matter density at redshift z, δ_g is the gas overdensity and X is the hydrogen mass fraction. We choose two values for this entropy floor, $S_{fl} = 50$ and 100 keV cm^2, that bracket the observed values in small groups and clusters (Ponman et al. 1999; Lloyd-Davies et al. 2000).

We assume $z_h = 3$ for the reference heating redshift, since it is close to the epoch at which sources of heating, such as SN or active galactic nuclei (AGN), are expected to reach their maximum activity (see below). At $z = 3$, we select all the gas particles with overdensity $\delta_g > 5$, so that they correspond to structures, which have already undergone turnaround. After assuming a minimum floor entropy, S_{fl}, each gas particle having $s_i < S_{fl}$ is assigned an extra thermal

energy, so as to bring its entropy to the floor value. We estimate the amount of energy injected in the ICM in these pre-heating schemes by selecting at $z = 0$ all the gas particles within the virial radius and tracing them back to $z = 3$. We find that taking $S_{\rm fl} = 50$ keV cm^2 amounts to give an average extra heating energy of $E_{\rm h} = \frac{3}{2} T_{\rm h} \simeq 1.4$ keV particle^{-1} for particles that end up within the virial radius of the Fornax and Hickson groups at $z = 0$, and $E_{\rm h} \simeq 0.9$ keV particle^{-1} for the Virgo cluster and $E_{\rm h} \simeq 0.8$ keV particle^{-1} for the Coma cluster. Such values are twice as large for $S_{\rm fl} = 100$ keV cm^2.

In the semi-analytical model by TN01, the gas is assumed not to have undergone any significant gravitational shock heating before $z_{\rm h}$, so that equation (9) actually gives the extra energy to be provided to the gas particles to bring them to the appropriate adiabat. The hierarchical clustering scenario, instead, predicts that a significant amount of non-linear structure already exists at $z_{\rm h} = 3$, with gas particles raised by gravitational shocks to an entropy level already higher than the floor to be set. In our heating scheme, the thermal energy of such particles is left unchanged.

This heating scheme can be defined as an external one, in the sense that it is also targeted at particles not belonging to collapsed structures. In principle this may violate constraints on the entropy of the diffuse high-z IGM, as inferred from observations of Ly-α absorption systems. If we identify a Ly-α system as a structure with typical gas overdensity $\delta_{\rm g} \simeq 30$, it has at $z = 3$ a temperature of $T \simeq 2.5 \times 10^{-3}$ keV, as determined by the condition of ionization equilibrium with the UV background (e.g. Haardt & Madau 2001). This corresponds to a typical entropy $S \simeq 5$–10 keV cm^{-2}, thus about an order of magnitude smaller than that relevant for ICM heating. Therefore, an external heating such as that imposed in our simulations would destroy Ly-α absorbers. In this sense, setting an entropy floor must just be considered as an approach guided by ICM phenomenology rather than motivated by general astrophysical arguments.

Even in this simple heating scenario, a further parameter is represented by the epoch at which the entropy floor is created. As the heating redshift is changed, two opposite effects compete in determining the energy budget required to create a given entropy floor. On the one hand, the higher $z_{\rm h}$ is, the smoother the particle distribution, the smaller the number of particles at high $\delta_{\rm g}$, which require a lot of heating to increase their entropy to the desired level. On the other hand, the higher $z_{\rm h}$, the higher the overall cosmic mean density $\bar{\rho}(z)$, the smaller the amount of heating energy needed at fixed $\delta_{\rm g}$. We check the effect of changing $z_{\rm h}$ by also running low-resolution simulations of the Fornax group with $z_{\rm h} = 1$, 2 and 5. In the following we will discuss the effect of changing $z_{\rm h}$ on the final results. The heating energies corresponding to the different $z_{\rm h}$ are shown in the top panel of Fig. 13 (see Section 4.4).

3.2 Energy feedback from supernovae

This pre-heating scheme is based on computing the star formation rate within clusters as predicted by a semi-analytic model of galaxy formation, a technique first introduced by White & Frenk (1991), Kauffmann, White & Guiderdoni (1993) and Cole et al. (1994), and subsequently adopted and developed by several authors (e.g. Somerville & Primack 1999; Cole et al. 2000; Wu et al. 2000). Here we use a variation of the scheme described by Menci & Cavaliere (2000), and we refer to this paper for a detailed description of the method.

In our approach, the merging history of dark matter haloes, having the same mass as the simulated ones, is predicted according to the extended Press–Schechter theory (EPST, e.g. Lacey & Cole 1993).

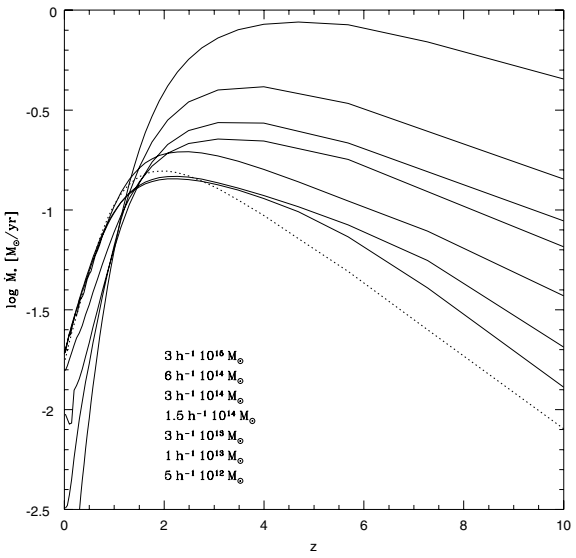

Figure 6. The integrated star formation rate for the condensations ending up in a present-day structure of mass M_0 is plotted as a function of redshift for the different values of M_0 shown in the labels. For comparison, the dotted curve shows the cosmic star formation rate predicted by our semi-analytical scheme. This figure can be seen in colour on *Synergy*, in the online version of the journal.

The processes of gas cooling, star formation and stellar feedback within galaxy-sized structures are described by means of a suitable parametrization of the corresponding star formation rate and reheated mass, which is ejected back into the hot diffuse medium. The free parameters of the model are chosen so as to reproduce observed properties of the local galaxy population (Tully–Fisher relation, *B*- and *K*-band luminosity functions, disc sizes).

In Fig. 6 we show the integrated star formation history $\dot{m}_*(z, M_0)$ of all the condensations that are incorporated into a structure of total mass M_0 by the present time. The curves in Fig. 6 correspond to M_0 values, which span the whole range from galaxies to rich clusters. As M_0 grows the local star formation rate (SFR) decreases, while the value at $z \gtrsim 2$ increases and its peak is attained at higher redshift. This is expected in the hierarchical clustering picture, since more massive structures originate from more biased regions, where initially the star formation rate was higher. The large consumption of cold baryons in the progenitors of M_0 at large z results in a smaller amount of available star-forming gas at small z, yielding the sharply declining $\dot{m}_*$ at $z \to 0$.

After assuming a Salpeter initial mass function (Salpeter 1955), the SFRs are then used to derive the SN heating appropriate to each system that we simulate, based on its virial mass. During the evolution of each halo, this energy is shared among all the gas particles having $\delta_{\rm g} > 50$. This overdensity threshold, which roughly corresponds to the density contrast at the virial radius, guarantees that gas heating takes place inside virialized regions. We verified that the final results do not change if only gas particles with $\delta_{\rm g} > 500$ are heated. Under the extreme assumption that all the energy released by SN is thermalized into the ICM (i.e. $\eta = 1$ for the SN efficiency) this scheme dumps a total amount of about 0.35 keV per gas particle. For the Hickson group we also run two more simulations with $\eta = 0.1$ and 4. In the first case, the energy budget is so small that the final results are essentially indistinguishable from the GH run (see Table 2) and, therefore, we will not comment further on this low-efficiency case. As for the second case, it corresponds to an amount

of extra energy similar to that of the S-50 entropy floor. This allows us to check whether the final results depend on the way in which a fixed amount of energy is dumped into the diffuse medium. Such a large amount of energy can be interpreted as being associated with any heating source, the evolution of which follows that of the SFR. This is likely to be the case for AGNs, whose emissivity per unit volume has been suggested to evolve according to the SFR (e.g. Cavaliere & Padovani 1989; Boyle & Terlevich 1998; Franceschini et al. 1999).

A word of caution should be mentioned here concerning our implementation of SN heating. We assume that all SNe release a fixed amount of energy, $E_{\rm SN} = 10^{51}$ erg. In the so-called hypernovae scenario, energies larger by at least one order of magnitude may be expected (e.g. Loewenstein 2001).

Furthermore, in our scenario only Type II SN are included, while Type Ia SN may in principle give a significant contribution to the ICM energetics (e.g. Pipino et al. 2002). Also, most of our simulations assume no radiative losses in SN explosions, so that the released energy is all thermalized in the ICM, which is a reasonable approximation if most of the SN explode in a hot and rarefied medium. Finally, the feedback used in the semi-analytical modelling of galaxy formation is not the same as that adopted for heating gas particles in the simulations. For all of these reasons, we tend to consider our SN heating scheme as a realistic but approximate recipe for estimating the amount of energy expected from a stellar population, rather than a self-consistent approach to including the effect of SN explosions on the ICM energetics.

4 RESULTS

4.1 Gas-density and temperature profiles

A unique signature of the lack of self-similarity in galaxy clusters is provided by the different profiles of gas density observed for clusters of different temperatures (e.g. Ponman et al. 1999; Lloyd-Davies et al. 2000), with colder systems having shallower internal profiles. In the upper panels of Fig. 7 we show how extra heating can affect the gas profiles. In the absence of any extra heating, all the simulated structures display the same gas density profile. This result agrees with the expectation of the self-similar scaling paradigm and confirms that non-linear gravitational processes, such as accretion shocks, do not introduce any characteristic scale. The only structure slightly deviating from self-similarity in the GH runs is the Coma cluster. Looking at its evolution, it turns out that this structure underwent a very recent major merger event, which redistributed the gas in the central regions. Therefore, its slightly softer gas profile is just the signature of this recent merger.

Self-similarity is broken as additional heating is included. SN feedback has some effect only on the gas profile for the Hickson group, our less massive halo. This is in line with the expectation that ICM thermodynamics ought to be changed only when the non-gravitational heating is comparable to the gravitational one. In fact, SN heating provides $\sim 1/3$ keV per gas particle, which is similar to the mass-weighted temperature of the Hickson group. As for the S-50 runs, the entropy floor corresponds to a large enough heating that only the Coma cluster remains almost unaffected. This result is in line with that based on the shape of entropy profiles presented in Paper I.

A relevant quantity that is directly related to the gas profile is the baryon fraction, $f_{\rm bar}$, within a given radius. The measurement of the baryon fraction in clusters, in combination with constraints on $\Omega_{\rm b}$ from primordial nucleosynthesis, is considered as one of the fundamental tests for the density parameter Ω_m (e.g. White, Efstathiou & Frenk 1993; Evrard 1997; Ettori 2002). We show in Fig. 8 the radial dependence of $f_{\rm bar}$ for the Virgo and Hickson runs with the different heating schemes. If gas is only subject to gravitational heating, the cosmic baryon fraction is recovered at about 0.3–0.4$R_{\rm vir}$, which is comparable to the effective scale where $f_{\rm gas}$ is determined from X-ray data. As for the Virgo cluster, the S-50 scenario would lead only to a $\sim$10–15 per cent underestimate of the correct value at about half the virial radius. The situation is quite different for the Hickson group, for which the gas fraction is diminished out to the virial radius by heating from the entropy floors. This provides a warning concerning the determination of $f_{\rm gas}$ and the inference of Ω_m based on poor clusters and groups. The heating from the SN scheme with 400 per cent efficiency (SN-4) produces an $f_{\rm gas}$ profile

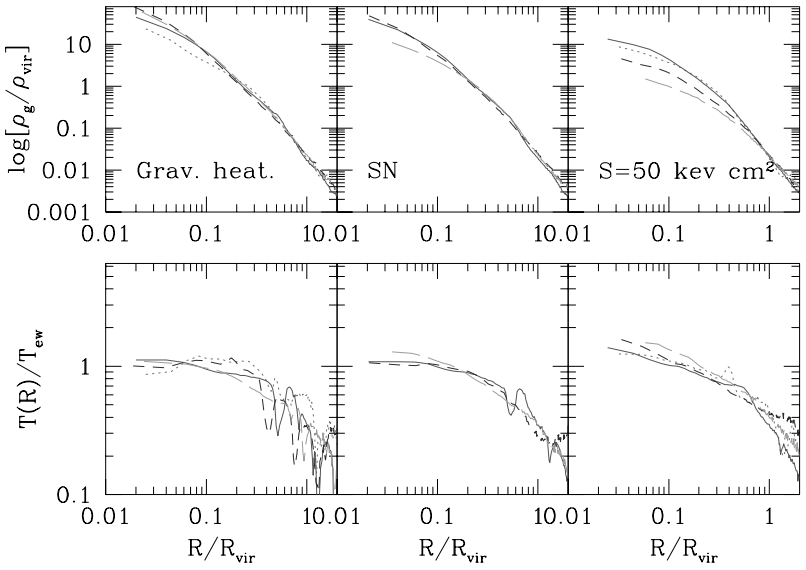

Figure 7. Profiles of gas density in units of the virial density (upper panels) and temperature in units of $T_{\rm ew}$ (lower panels) at $z = 0$. Left, central and right-hand panels are for the GH, SN and S-50 runs, respectively. Dotted, solid, short-dashed and long-dashed curves refer to the Coma, Virgo, Fornax and Hickson runs, respectively. This figure can be seen in colour on *Synergy*, in the online version of the journal.

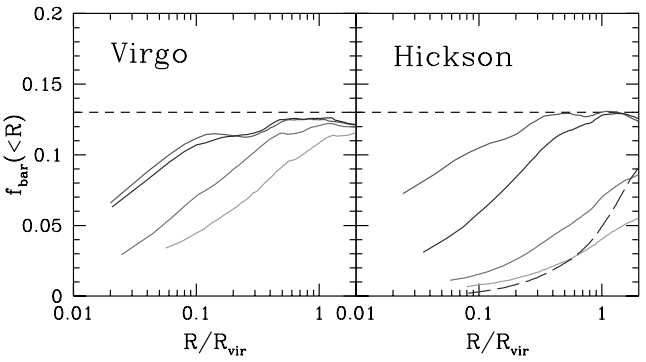

Figure 8. Profiles of the baryon fraction within a given radius for Virgo and Hickson runs. Gravitational heating, SN feedback, and entropy floors with $S = 50$ and 100 keV cm^2 are shown from upper to lower solid curves. The dashed curve for the Hickson run indicates the SN heating scheme with efficiency raised to 400 per cent (SN-4). The horizontal dashed line indicates the cosmic baryon fraction. This figure can be seen in colour on *Synergy*, in the online version of the journal.

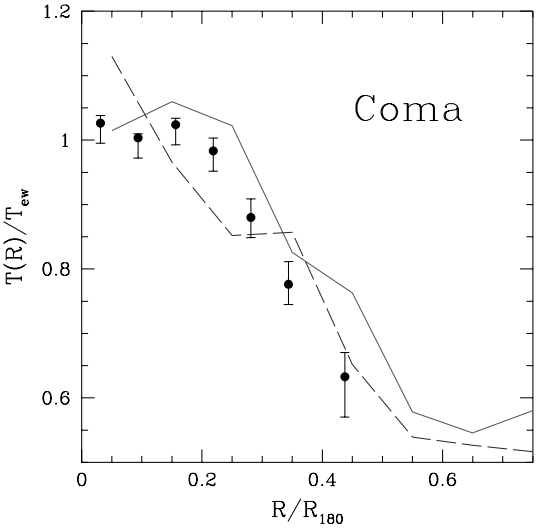

Figure 9. The projected temperature profile for the GH and S-50 Coma runs (solid and dashed lines, respectively), compared with the average temperature profile for the set of 21 clusters observed with Beppo-SAX and analysed by De Grandi & Molendi (2002). Simulation results are obtained by averaging the profiles obtained by projecting along three orthogonal directions. The cluster-centric radius is expressed in units of R_{180}, which is defined as the radius encompassing the density $180\rho_{crit}$. This figure can be seen in colour on *Synergy*, in the online version of the journal.

quite similar to the S-100 scheme within the virial radius. Quite interestingly, the S-100 scheme involves an extra-heating energy, $E_h \simeq 2.8$ keV, which is almost twice as large as for the former scheme. This indicates that a redshift-modulated heating is more efficient, in terms of the required energy budget, than an impulsive pre-collapse heating.

As for the three-dimensional temperature profiles (lower panels of Fig. 7), the gas looks almost isothermal, in the absence of any extra heating, out to $\sim 0.2\ R_{vir}$, while a fairly steep gradient appears at larger radii. Dips in the T-profiles indicate the presence of merging structures, for which lower virial temperature brings colder gas in the main body of the simulated system, before being stripped by ram pressure and thermalized. Such structures are progressively washed out in the pre-heated runs, as a consequence of the smaller amount of gas that subgroups are able to keep in such cases. The extra heating also steepens the temperature profiles in the internal cluster regions, with a more pronounced gradient for smaller systems. An increase of gas temperature in the central regions is a consequence of suppressing the gas density while keeping the external gas pressure unchanged.

Over the last few years, observational data have reached good enough precision to allow for spatially resolved spectroscopic observations of the ICM for a fair number of galaxy clusters. Yet, a general agreement concerning the temperature profiles in the external cluster regions, not affected by cooling, has still to be reached (e.g. Markevitch et al. 1998; White 2000; Irwin & Bregman 2000). Based on Beppo-SAX observations, De Grandi & Molendi (2002) analysed projected temperature profiles for a set of 21 clusters. They found the gas to be isothermal out to $\sim 0.2 R_{180}$, with a fairly steep negative gradient at larger radii. In Fig. 9 we compare results from our simulations with the average profile by De Grandi & Molendi (2002). Since their clusters are all quite hot ($T \gtrsim 4$ keV), we use only results from the Coma run. The simulation results are obtained by averaging over the temperature profiles projected along three orthogonal directions. The simulation produces a fairly steep gradient at $R \gtrsim 0.2 R_{180}$, quite similar to the observed one. Forthcoming data from *Chandra* and *Newton–XMM* (e.g. Arnaud et al. 2001; Allen, Schmidt & Fabian 2001) will certainly refine the determination of temperature profiles in central cluster regions, where cooling is also expected to play a significant role. There is no doubt that such observational advances will challenge the ability of numerical simulations to treat the relevant physical processes.

4.2 The mass–temperature relation

The M–T relation represents a key ingredient when comparing observational data on the cluster X-ray temperature function with the mass function predicted by cosmological models. Quite recently, the different results obtained by different authors on the power-spectrum normalization, σ_8, from cluster XTF and XLF have lead to a discussion on the correct M–T relation to be used (e.g. Pierpaoli, Scott & White 2001; Borgani et al. 2001b; Seljak 2002; Viana, Nichol & Liddle 2002; Ikebe et al. 2002). In past years, different analyses have shown that equation (3) provides a good fit to results of simulations including only gravitational heating, with values of β ranging within the interval $0.9 \lesssim \beta \lesssim 1.3$ (e.g. Evrard, Metzler & Navarro 1996, E96 hereafter; Bryan & Norman 1998; Frenk et al. 2000). In particular, E96 pointed out that temperature measurements provide a quite accurate determination of the mass at radii where the mean cluster density is 500–$2500\rho_{crit}$.

Besides investigating the effect of non-gravitational heating on the M–T relation, the excellent resolution of our simulations allow one to better resolve the structure of cluster cores, which is relevant for determinations of the emission-weighted temperature. Results on the M_{vir}–T_{mw} relation from our simulations (left-hand panel of Fig. 10) closely follow the relation of hydrostatic equilibrium of equation (3) with a very small scatter and almost no dependence on non-gravitational heating. Although extra heating adds internal energy to the gas particles, they quickly get back in hydrostatic equilibrium, with their temperature being determined by the depth of the gravitational potential well, which is established by the dynamically dominant DM component.

As for observational data, determinations of the M–T relation have been realized over the last few years by different groups using *ASCA*

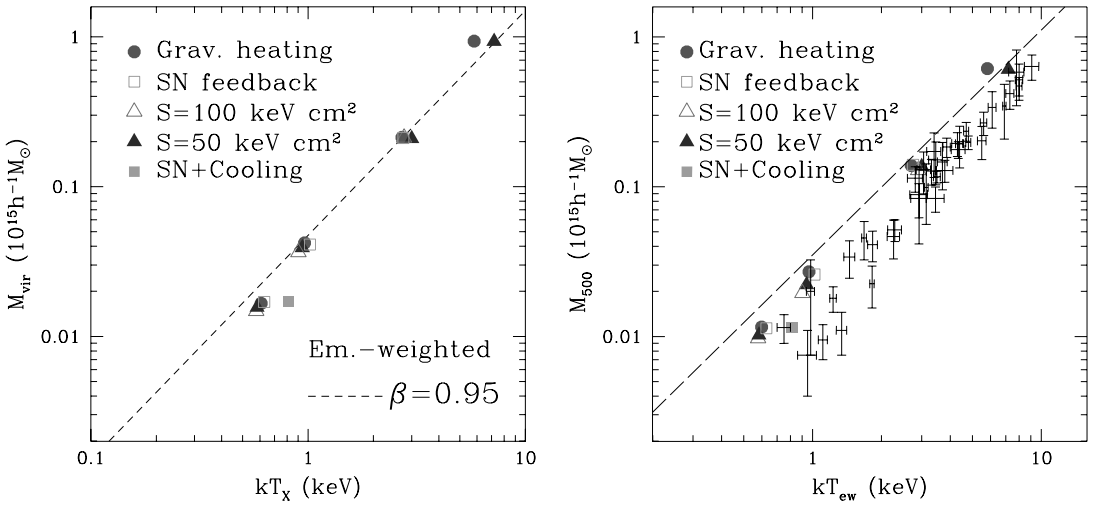

Figure 10. Left-hand panel: the relation between total virial mass and emission-weighted temperature for simulated clusters. The dashed line shows the relation of equation (3), with normalization as given by the reported β values. Right-hand panel: the relation between mass estimated at r_{500} and emission-weighted temperature. Dotted crosses are the observational results by F01. The dashed line shows the best-fitting relation found by Evrard et al. (1996). This figure can be seen in colour on *Synergy*, in the online version of the journal.

(Horner, Mushotzky & Scharf 1999; Nevalainen, Markevitch & Forman 2000; Finoguenov, Reiprich & Böhringer 2001, F01 hereafter) and Beppo-SAX data (Ettori, De Grandi & Molendi 2002). Such analyses consistently find that (i) $M \propto T^{3/2}$ for $T \gtrsim 4$ keV, but with a normalization significantly lower than that found by E96 from simulations (cf. Ettori et al. 2002) and (ii) a steeper slope for colder systems, possibly interpreted as an effect of pre-heating. In the right-hand panel of Fig. 10 we compare data on the M_{500}–$T_{\rm ew}$ relation by F01, which include data on systems down to $T_{\rm ew} \lesssim 1$ keV, to results from our simulations and to the relation found by E96. The somewhat lower normalization with respect to the E96 results on the group scale is likely to be a result of our improved resolution. However, the effect of extra heating is at most marginal and not sufficient to reconcile simulations to data, thus indicating that some other physical process should be at work in establishing the M–T scaling.

F01 suggest that the difference between the observed and the simulated M–T relation is caused by the combined effect of pre-heating and the effect of formation redshift on the temperature of the system. However, our simulations show that pre-heating has a minor impact on this relation. As for the effect of formation redshift, it may introduce a bias in the definition of the observational data set: observations could tend to select fairly relaxed systems, which formed at higher redshift and, therefore, are characterized by a somewhat higher temperature at a fixed mass (e.g. Kitayama & Suto 1996; Voit & Donahue 1998). Our simulations define an M–T relation with a small scatter, thus suggesting that differences in the formation epoch or differences in the current dynamical status among systems should have a small effect. A larger set of simulated clusters would be required to properly address this point. Ettori et al. (2002) detect a segregation in the M–T relation for cooling-flow and non-cooling-flow clusters, the latter being characterized by a larger scatter.

TN01 showed that their ICM model, which incorporates the effects of pre-heating and cooling, reproduces the observed M–T relation. They also find that the predicted relation is weakly sensitive to the value of the pre-collapse entropy floor. This suggests that cooling should be responsible for the lower normalization of the relation, through the steepening of the temperature profiles in cluster central regions. The effect of cooling on the M–T relation will be discussed further in Section 5 below.

4.3 The luminosity–temperature relation

The observed relation between bolometric luminosity and temperature is considered a standard argument against the self-similar behaviour of the ICM. Bremsstrahlung emissivity predicts $L_{\rm X} \propto M\rho_{\rm gas}T^{1/2}$. Therefore, as long as clusters of different mass are scaled versions of each other, then the M–T scaling from hydrostatic equilibrium gives $L_{\rm X} \propto T_{\rm X}^2(1+z)^{3/2}$ or, equivalently $L_{\rm X} \propto M^{4/3}(1+z)^{7/2}$ for $\Omega_m = 1$ (Kaiser 1986; see Eke et al. 1998, for an extension to low-Ω_m cosmologies). As we also discussed in the introduction, this prediction is at variance with respect to observational evidence of a steeper relation, $L_{\rm X} \propto T^{\sim 3}$ for $T \gtrsim 2$ keV and, possibly, even steeper for colder systems. This result is also in line with the observed slope of the $L_{\rm X}$–M relation, $L_{\rm X} \propto M^{\alpha}$ with $\alpha \simeq 1.8 \pm 0.1$ (Reiprich & Böhringer 2002).

The first determinations of the $L_{\rm X}$–T relation for clusters showed that it has a quite large scatter (e.g. David et al. 1993; White et al. 1997). A significant part of this has been recognized to be the effect of cooling: central spikes associated with cooling regions provide a large fraction of total X-ray luminosity, so that differences in the cooling structure among clusters of similar temperature induce a spread in the corresponding $L_{\rm X}$ values. After correcting for this effect, different authors (Allen & Fabian 1998; Markevitch 1998; Arnaud & Evrard 1999) were able to calibrate a much tighter $L_{\rm X}$–T relation. Allen & Fabian (1998) also noticed that the $L_{\rm X}$–T relation for the hottest clusters tends to flatten to the self-similar scaling prediction, possibly suggesting that the effect of extra heating becomes negligible for such systems.

Fig. 11 shows the effect of extra heating on the $L_{\rm X}$–T relation of nearby clusters. The GH runs are clearly at variance with respect to data over the whole sampled range of temperatures. Heating with the SN-1 recipe provides some steepening of the $L_{\rm X}$–T relation at the group scale, although not enough to reach agreement with data points. A larger suppression of $L_{\rm X}$ is achieved with the S-50 and S-100 heating schemes and, for the Hickson group, with the SN-4 run. Quite interestingly, the SN-4 heating scheme requires the same

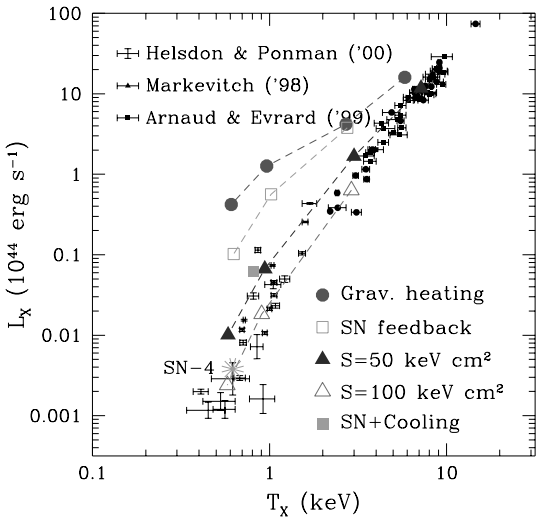

Figure 11. The relation between X-ray luminosity and emission-weighted temperature at $z = 0$. Results from simulations are compared with observational data for nearby clusters (data points with error bars) from different authors. The asterisk indicates the SN-4 Hickson run, which corresponds to $E_h = 1.4$ keV particle^{-1} for the heating energy. This figure can be seen in colour on *Synergy*, in the online version of the journal.

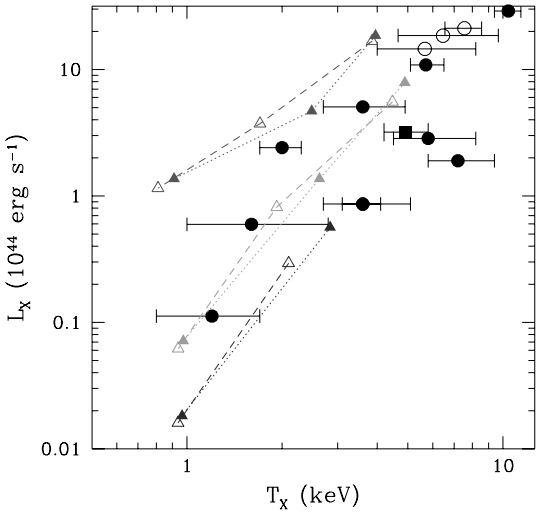

Figure 12. The L_X–T relation for distant $z \geqslant 0.5$, clusters. Triangles connected by lines are simulation results for Coma, Virgo and Fornax runs at $z = 0.5$ (filled triangles with dotted lines) and $z = 1$ (open triangles with dashed lines). The three groups of simulation results at decreasing L_X refer to the GH, S-50 and S-100 runs (for reasons of clarity we do not include the case of SN feedback). Data points with error bars refer to $z > 0.5$ clusters from Beppo-SAX and *ASCA* data (Della Ceca et al. 2000, open circles), Chandra data extending out to $z = 1.27$ (Borgani et al. 2001b; Stanford et al. 2002, filled circles) and from the *XMM* observation of the $z = 1.26$ cluster of the Lockman hole (Hashimoto et al. 2002, square). This figure can be seen in colour on *Synergy*, in the online version of the journal.

heating energy, $E_h \simeq 1.4$ keV particle^{-1} as the S-50 entropy floor, but provides a significantly smaller luminosity, as a consequence of the lower gas density in the central region of the Hickson group (see also Fig. 8). Therefore, a better efficiency is reached in this case by gradually dumping energy within the virialized regions of the ICM, rather than imposing an impulsive pre-collapse heating on the whole turnaround region.

In a similar way, Fig. 12 shows a similar comparison with observations for distant, $0.5 \lesssim z \lesssim 1.3$, clusters. Independent analyses have confirmed that data on the L_X–T relation of distant clusters are consistent with a lack of evolution (e.g. Mushotzky & Scharf 1997; Donahue et al. 1999; Della Ceca et al. 2000; Borgani et al. 2001b; Holden et al. 2002; Stanford et al. 2002). Since no data are available on $T \lesssim 1$ keV groups in the above z-range, we do not include in this comparison results for the Hickson runs. Although temperature determinations for distant clusters are prone to larger error bars, the results are quite in line with what is shown in Fig. 11: the L_X–T relation of distant clusters requires pre-heating of the ICM with $E_h \gtrsim 1$ keV particle^{-1}.

4.4 The effect of changing the epoch of heating

Imposing an entropy floor at some pre-collapse redshift is a useful approximation, in that it allows the characterization of the ICM evolution by a single quantity, which is conserved in adiabatic processes. As already mentioned, the heating energy required to establish a given entropy floor is a non-trivial function of the heating redshift, z_h, through the evolution of $\bar{\rho}$ and δ_{gas} (see equation 9). In general, one may also expect the resulting global ICM properties to depend on z_h. In their simulations, Bialek et al. (2001) heated at a very high redshift, $z_h \sim 20$, and found results on the required S_{fl} to reproduce the observed L_X–T relation that are generally consistent with ours. This may suggest that the choice for z_h is not relevant. However, a close comparison between their runs and ours is not straightforward: mass and dynamical resolutions are higher in our runs and, as discussed in Section 2, this is likely to affect observable quantities, such as L_X, which are sensitive to the details of gas clumpiness.

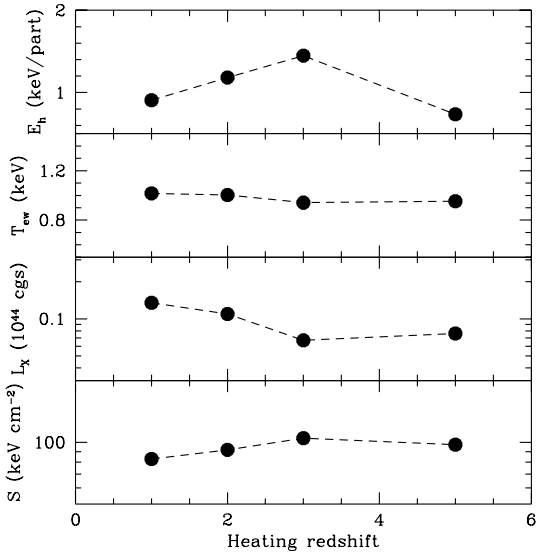

Figure 13. The effect of changing the heating redshift, z_h, for the low-resolution S-50 Fornax run. Results are shown for the specific heating energy, the emission-weighted temperature, the X-ray luminosity and the entropy at $0.1R_{vir}$ (from upper to lower panels).

As shown in Fig. 13, the required E_h for the S-50 Fornax run changes by about a factor of 2, $z_h = 3$ being the less efficient choice in terms of energy budget. Both T_{ew} and the central gas entropy at $0.1R_{vir}$ are quite stable, with variations of at most ∼10 and ∼20 per cent, respectively. As expected, the X-ray luminosity is the most

sensitive quantity to changes of z_h; it decreases by about a factor of 2 as the heating epoch is pushed back in time from $z_h = 1$ to 5. Such relatively modest variations suggest that different choices for z_h induce only moderate changes in the value of S_{fl} required to reproduce the observed L_X–T relation.

5 THE EFFECT OF COOLING AND STAR FORMATION

The simulations discussed so far have been realized with the aim of understanding in detail the effect of non-gravitational heating on ICM observable quantities. However, excluding cooling in our simulations is clearly a simplification, and its inclusion is likely to change some results significantly. Cooling times can be significantly shorter than the Hubble time in central regions of clusters, thus causing a significant fraction of the gas there to cool down and drop out of the hot diffuse, X-ray-emitting phase (see Fabian 1994, for a review on cooling processes in clusters).

Cooling has been suggested as an alternative to non-gravitational heating for breaking ICM self-similarity. As gas undergoes cooling in central cluster regions, X-ray luminosity is suppressed as a consequence of the reduced amount of diffuse hot gas (Pearce et al. 2000), thus possibly producing a steepening of the L_X–T relation (Muanwong et al. 2001; Wu & Xue 2002). The decreased pressure support causes the recently shocked, higher-entropy external gas to flow in, thus causing a net increase of entropy for the hot gas left in central cluster regions (Bryan 2000). Recently, Voit & Bryan (2001) have argued that only gas with entropy in excess of 100–200 keV cm^2 has a long enough cooling time to remain in the diffuse phase. Accordingly, the entropy excess in central regions of poor groups should be interpreted as an effect of cooling, rather than of extra heating.

In order to check this effect, we realized a high-resolution run of the Hickson group, with the SN-1 heating scheme, but also including gas cooling. The cooling function adopted assumes gas of primordial composition, with zero metallicity, and follows the recipe of Wadsley & Bond (1997). We also include heating by the UV background by adopting the latest version of the model by Haardt & Madau (2001). We follow the recipe by Katz, Hernquist & Weinberg (1992) to convert dense cold gas particles into collisionless stars. Furthermore, when computing properties of the diffuse ICM, we exclude gas particles with temperatures $T < 3 \times 10^4$ K and overdensities $\delta > 500$ (see also Kay et al. 2002). These particles are assumed to belong to the cold medium, although not yet removed from the gas phase by the star formation (SF) algorithm. The effect of including cooling and SF is that of collecting gas into dense knots, while suppressing gas density in the diffuse filamentary structures (see Fig. 14). The resulting density profile in central regions turns out to be steeper, $\propto R^{-\alpha}$, with $\alpha \simeq 2$ than that for a CDM-only run (see also Treu & Koopmans 2002).

In Fig. 15 we show the resulting entropy profile, as compared with the GH and SN-1 runs, with no cooling. We detect some increase of gas entropy inside R_{vir}, owing to the infall of shocked external gas. However, the inclusion of cooling and SF do not produce any entropy plateau at $\sim$100 keV cm^2. Although the entropy increase goes in the right direction, it may be marginal in accounting for the observed entropy excess in central group regions (e.g. Ponman et al. 1999, see also Paper I). A higher entropy could possibly be attained by assuming a non-negligible metallicity in the cooling function, which would cause an increasing in efficiency of gas cooling.

Besides suppressing the amount of hot X-ray-emitting gas, cooling also causes the formation of high-density concentrations of star particles in the innermost cluster region. Such concentrations deepen the potential well and cause the temperature there to increase significantly. Therefore, while the X-ray luminosity decreases, the emission-weighted temperature increases. The effect of cooling in the M–T_{ew} and L_X–T relations of the Hickson run is shown with the filled square in Figs 9–11 . Such changes actually go in the right direction for improving the L_X–T relation (see Fig. 11) and possibly solve the discrepancy with the observed M_{500}–T_{ew} relation (see also Thomas et al. 2002; Voit et al. 2002).

However, cooling in itself is a runaway process, owing to the quick increase of cooling efficiency with local gas density. Consequently, if not counteracted by some feedback process, a too large fraction of

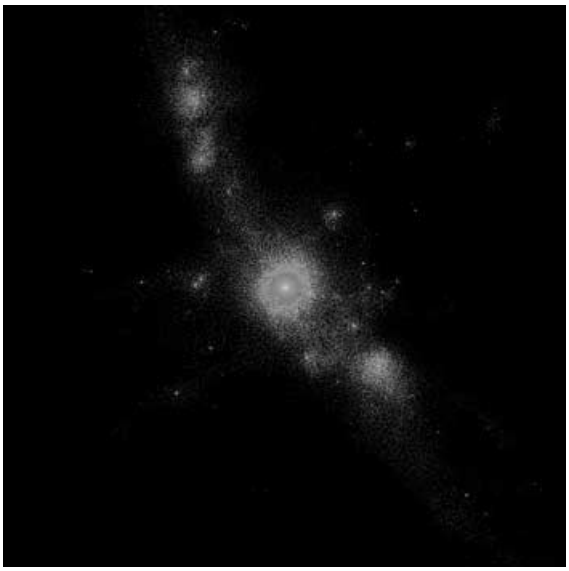

Figure 14. The map of the gas density for the SN-1 Hickson run including cooling and star formation. The box size is the same as in Fig. 2. This figure can be seen in colour on *Synergy*, in the online version of the journal.

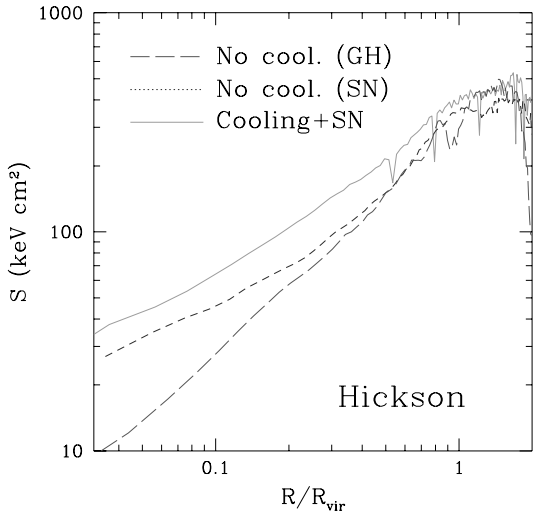

Figure 15. The entropy profiles for the Hickson simulation without cooling (for the GH and SN-1 cases) and including the effect of cooling and star formation in the SN-1 run. In the computation of the entropy for the cooling run, only gas particles belonging to the hot diffuse phase have been considered (see text). This figure can be seen in colour on *Synergy*, in the online version of the journal.

gas can cool down to a collisionless phase (e.g. Prunet & Blanchard 1999; Lewis et al. 2000; Balogh et al. 2001; Davé et al. 2001). We see in our simulation that while the overall baryonic fraction inside $R_{\rm vir}$ at $z = 0$ coincides with the cosmic value, 37 per cent of the gas is locked in the stellar phase. This large fraction is far in excess of the $\lesssim$10 per cent fraction indicated by observations (e.g. Balogh et al. 2001). Therefore, our SN feedback scheme falls short of preventing the cooling runaway.

Addressing in detail the issue of preventing overcooling through a suitable feedback mechanism is beyond the scope of this paper. Owing to the biased nature of halo formation in hierarchical models, the first massive haloes to collapse into a protocluster region will eventually merge to form its core. These massive haloes host the progenitors of giant ellipticals in present-day clusters (Governato et al. 2001; Springel et al. 2001) and will probably contribute to most of the energy released in the ICM. Whatever the astrophysical source for this energy is, it should act in a self-regulated way: cooling switches on the feedback mechanism and the subsequent energy release inhibits too much gas to leave the hot phase. Besides SN, also AGN activity has been suggested as a possible way of preventing overcooling, with energy released with a duty cycle of a few 10^7 yr (e.g. Binney & Tabor 1995; Ciotti & Ostriker 2001; Quilis, Bower & Balogh 2001; Böhringer et al. 2002). If AGN are responsible for the required feedback, then one should expect to see some signature of their recent activity in the central regions of those clusters, for which cooling has been recently switched off. A successful and self-consistent inclusion of cooling and feedback in numerical simulations has still to be realized, with the main difficulty lying in the treatment of physical processes, which involve a large dynamical range. The physics describing AGN activity or SN explosions involve small scales that are out of the reach of current and foreseeable simulations of galaxy clusters, thus leaving as the only possibility the inclusion of such process as external recipes.

6 CONCLUSIONS

We have presented results from high-resolution Tree+SPH simulations of galaxy clusters and groups aimed at studying the effect of non-gravitational heating of the intracluster medium on observable X-ray properties of galaxy systems. Four simulated structures have been chosen so as to encompass the temperature range from a poor Hickson-like group to a rich Coma-like cluster. Two different kinds of non-gravitational gas heating have been chosen: (i) impulsive heating to set an entropy floor at some redshift ($z_{\rm h} = 3$ as a reference epoch); (ii) gradual heating, which follows the star formation rate inside the cluster region, as predicted by semi-analytical modelling of galaxy formation, so as to mimic the effect of SN energy feedback. Our main results can be summarized as follows.

(a) In order for simulations to reproduce analytical predictions for the $L_{\rm X}$–T relation of gas sitting in hydrostatic equilibrium within a NFW potential well, the structure of the gas distribution needs to be resolved with at least 5–10 $\times$ 10^4 gas particles within the virial radius, with a spatial resolution of the order of 1–2 per cent of $R_{\rm vir}$.

(b) The observed slope and amplitude of the $L_{\rm bol}$–$T_{\rm ew}$ relation are well reproduced by setting an entropy floor of 50–100 keV cm^2. Assuming negligible radiative losses, SN feedback provides $\simeq$0.35 keV particle^{-1} and, as such, has a too small effect on the $L_{\rm X}$–T relation. A four times larger energy, possibly consistent with that obtainable from AGN, is required to reproduce the $L_{\rm X}$–T relation at the scale of a Hickson group.

(c) In the absence of cooling, the M_{500}–$T_{\rm ew}$ relation is found to be higher by $\simeq$40 per cent than that observed, over the whole sampled T range, almost independent of the presence and amount of non-gravitational heating. Therefore, non-gravitational heating in itself is not able to account at the same time for the $L_{\rm bol}$–$T_{\rm ew}$ and the M_{500}–$T_{\rm ew}$ relations.

(d) The effect of including cooling in the simulation of a Hickson group with SN heating is to suppress $L_{\rm X}$ by about 40 per cent and to increase $T_{\rm ew}$ by about 30 per cent. Therefore, the effect of cooling goes in the right direction of decreasing the amplitude of the $L_{\rm X}$–T and M_{500}–$T_{\rm ew}$ relations at the scale of groups. However, the runaway nature of cooling is not efficiently counteracted by our SN feedback scheme, so that 37 per cent of the gas drops out of the hot X-ray-emitting phase. Such a large amount of cold gas is in contrast with observational data on the stellar content of galaxy systems.

The results presented in this paper demonstrate that no unique simple recipe exists to explain X-ray observable properties of galaxy systems. Supernova heating provides a sizeable, but insufficient, fraction of the non-gravitational heating energy required. Further feedback energy from AGN may be required. Yet, the mechanisms to thermalize the energy associated with QSO activity in the diffuse medium have to be understood in detail.

While much further work is needed, our study suggests that a combination of different heating sources (SN and AGN) *and* cooling will hopefully be able to reproduce *both* the correct $L_{\rm X}$–$T_{\rm ew}$ and M_{500}–$T_{\rm ew}$ relations, and to avoid gas overcooling. A self-consistent treatment of such complex physics is mandatory if the numerical description of the ICM has to keep pace with the progress in the observational description of the hot baryons in clusters.

ACKNOWLEDGMENTS

Simulations were run at the CINECA Supercomputing Centre, with CPU time provided by a grant of the Italian National Council for Astronomy and Astrophysics (CNAA). We thank the referee, Jerry Ostriker, for useful comments. We thank Fabrizio Brighenti and Mark Voit for a careful reading of the paper and Sabrina De Grandi and Alexis Finoguenov for providing us with the files of the data points shown in Figs 9 and 10, respectively. We acknowledge useful discussions with Richard Bower, Stefano Ettori and Colin Norman.

REFERENCES

Allen S.W., Fabian A.C., 1998, MNRAS, 297, 63
Allen S.W., Schmidt R.W., Fabian A.C., 2001, MNRAS, 328, L37
Anninos P., Norman M., 1996, 459, 12
Arnaud M., Evrard A.E., 1999, MNRAS, 305, 631
Arnaud M., Neumann D.M., Aghanim N., Gastaud R., Majerowicz S., Hughes J.P., 2001, A&A, 365, L80
Babul A., Balogh H.L., Lewis G.F., Poole G.B., 2002, MNRAS, 330, 329
Balogh M.L., Babul A., Patton D.R., 1999, MNRAS, 307, 463
Balogh M.L., Pearce F.R., Bower R.G., Kay S.T., 2001, MNRAS, 326, 1228
Bialek J.J., Evrard A.E., Mohr J.J., 2001, ApJ, 555, 597
Bingelli B., Tammann G.A., Sandage A., 1987, AJ, 94, 251
Binney J., Tabor G., 1995, MNRAS, 276, 663
Böhringer H., Matsushita K., Churazov E., Ikebe Y., Chen Y., 2002, A&A, 382, 804
Borgani S., Governato F., Wadsle J., Menci M., Tozzi P., Lake G., Quinn T., Stadel J., 2001a, ApJ, 559, L71 (Paper I)

Borgani S. et al., 2001b, ApJ, 561, 13
Bower R.G., 1997, MNRAS, 288, 355
Bower R.G., Benson A.J., Bough C.L., Cole S., Frenk C.S., Lacey C.G., 2001, MNRAS, 325, 497
Boyle B.J., Terlevich R.J., 1998, MNRAS, 293, L49
Briel U.G. et al., 2001, A&A, 365, L60
Brighenti F., Mathews W.G., 2001, ApJ, 553, 103
Bryan G.L., 2000, ApJ, 544, L1
Bryan G.K., Norman M.L., 1998, ApJ, 495, 80
Burles S., Tytler D., 1998, Space Sci. Rev., 84, 65
Cavaliere A., Padovani P., 1989, ApJ, 340, L5
Cavaliere A., Menci N., Tozzi P., 1998, ApJ, 501, 493
Cavaliere A., Menci N., Tozzi P., 1999, MNRAS, 308, 599
Ciotti L., Ostriker J.P., 2001, ApJ, 551, 131
Cole S., Aragon-Salamanca A., Frenk C.S., Navarro J.F., Zepf S.E., 1994, MNRAS, 271, 781
Cole S., Lacey C., Baugh C., Frenk C., 2000, MNRAS, 319, 168
Couchman H.M.P., 1991, ApJ, 368, 23
Davé R. et al., 2001, ApJ, 552, 473
David L.P., Slyz A., Jones C., Forman W., Vrtilek S.D., Arnaud K.A., 1993, ApJ, 412, 479
De Grandi S., Molendi S., 2002, ApJ, 567, 163
Della Ceca R., Scaramella R., Gioia I.M., Rosati P., Fiore F., Squires G., 2000, A&A, 353, 498
Donahue M., Voit G.M., Scharf C.A., Gioia I.M., Mullis C.R., Hughes J.P., Stocke J.T., 1999, ApJ, 527, 525
Drinkwater M.J. et al., 2000, A&A, 355, 900
Eke V.R., Cole S., Frenk C.S., 1996, MNRAS, 282, 263
Eke V.R., Navarro J., Frenk C.S., 1998, ApJ, 503, 569
Eke V.R., Navarro J., Steinmetz M., 2001, ApJ, 554, 114
Ettori S., 2002, MNRAS, 323, L1
Ettori S., Fabian A.C., 2001, in Matteucci F., Fusco-Femiano R., eds, Proceeding of the Vulcano Workshop on Chemical Enrichment of the Intracluster and Intergalactic Medium., p. 23
Ettori S., De Grandi S., Molendi S., 2002, A&A, in press (astro-ph/0206120)
Evrard A.E., 1997, MNRAS, 292, 289
Evrard A.E., Henry J.P., 1991, ApJ, 383, 95
Evrard A.E., Metzler C.R., Navarro J.F., 1996, ApJ, 469, 494 (E96)
Fabian A.C., 1994, ARAA, 32, 277
Fairley B.W., Jones L.R., Scharf C., Ebeling H., Perlman E., Horner D., Wegner G., Malkan M., 2000, MNRAS, 315, 669
Finoguenov A., Ponman T.J., 1999, MNRAS, 305, 325
Finoguenov A., Reiprich T.H., Böhringer H., 2001, A&A, 369, 479 (F01)
Finoguenov A., Jones C., Böhringer H., Ponman T.J., 2002, ApJ, in press (astro-ph/0206362)
Franceschini A., Hasinger G., Miyaji T., Malquori D., 1999, MNRAS, 310, L5
Frenk C.S. et al., 2000, ApJ, 525, 554
Geller M.J., Diaferio A., Kurtz M.J., 1999, ApJ, 517, L23
Ghigna S., Moore B., Governato F., Lake G., Quinn T., Stadel J., 2000, ApJ, 544, 616
Governato F., Ghigna S., Moore B., Quinn T., Stadel J., Lake G., 2001, ApJ, 547, 555
Haardt F., Madau P., 2001, in Neumann D.M. et al., eds, Proc. XXXVIth Rencontres de Moriond (astro-ph/0106018)
Hashimoto Y., Hasinger G., Aranud M., Rosati P., Miyaji T., 2002, A&A, 381, 841
Helsdon S.F., Ponman T.J., 2000, MNRAS, 315, 356
Holden B., Stanford S.A., Rosati P., Squires G.K., Tozzi P., Eisenhardt P., Elston R., 2002, ApJ, 124, 33
Horner D.J., Mushotzky R.F., Scharf C.A., 1999, ApJ, 520, 78
Ikebe Y., Reiprich T.H., Böhringer H., Tanaka Y., Kitayama T., 2002, A&A, 383, 773
Irwin J.A., Bregman J.N., 2000, ApJ, 538, 543
Kaiser N., 1986, MNRAS, 222, 323
Kaiser N., 1991, ApJ, 383, 104
Katz N., White S.D.M., 1993, ApJ, 412, 455
Katz N., Hernquist L., Weinberg D.H., 1992, ApJS, 105, 19
Kauffmann G., White S.D.M., Guiderdoni B., 1993, MNRAS, 264, 201
Kay S.T., Pearce F.R., Frenk C.S., Jenkins A., 2002, MNRAS, 330, 113
Kitayama T., Suto J., 1996, ApJ, 469, 480
Kravtsov A.V., Yepes G., 2000, MNRAS, 318, 227
Lacey C., Cole S., 1993, MNRAS, 262, 627
Lewis G.F., Babul A., Katz N., Quinn T., Hernquist L., Weinberg D.H., 2000, ApJ, 536, 623
Lloyd-Davies E.J., Ponman T.J., Cannon D.B., 2000, MNRAS, 315, 689
Loewenstein M., 2001, ApJ, 557, 573
Loewenstein M., Mushotzky R., 1996, ApJ, 466, 695
Markevitch M., 1998, ApJ, 504, 27
Markevitch M., Forman W.R., Sarazin C.L., Vikhlinin A., 1998, ApJ, 503, 77
Markevitch M. et al., 2000, ApJ, 541, 542
Mazzotta P., Markevitch M., Vikhlinin A., Forman W.R., David L.P., VanSpeybroek L., 2001, ApJ, 555, L87
McNamara B.R. et al., 2000, ApJ, 534, L135
Menci N., Cavaliere A., 2000, MNRAS, 311, 50
Mo H.J., Mao S., White S.D.M., 1998, MNRAS, 295, 319
Moore B., Governato F., Quinn T., Stadel J., Lake G., 1998, ApJ, 499, L5
Muanwong O., Thomas P.A., Kay S.T., Pearce F.R., Couchman H.M.P., 2001, ApJ, 552, L27
Mushotzky R.F., Scharf C.A., 1997, ApJ, 482, L13
Nath B.B., Roychowdhury S., 2002, MNRAS, 333, 145
Navarro J.F., Frenk C.S., White S.D.M., 1995, MNRAS, 275, 720
Navarro J.F., Frenk C.S., White S.D.M., 1997, ApJ, 490, 493 (NFW)
Neumann D.M., Arnaud M., 2001, A&A, 365, L80
Nevalainen J., Markevitch M., Forman W.R., 2000, ApJ, 536, 73
Pearce F.R., Thomas P.A., Couchman H.M.P., Edge A.C., 2000, MNRAS, 317, 1029
Pen U.-L., 1999, ApJ, 510, L1
Pierpaoli E., Scott D., White M., 2001, MNRAS, 325, 77
Pildis R.A., Bregman J.N., Evrard A.E., 1995, ApJ, 443, 514
Pipino A., Matteucci F., Borgani S., Biviano A., 2002, New Astron, 7, 227
Poli F., Giallongo E., Menci N., D'Odorico S., Fontana A., 1999, ApJ, 527, 662
Ponman T.J., Bourner P.D.J., Ebeling H., Böhringer H., 1996, 293, 690
Ponman T.J., Cannon D.B., Navarro J.F., 1999, Nat, 397, 135
Power C., Navarro J.F., Jenkins A., Frenk C.S., White S.D.M., Springel V., Stadel J., Quinn T., 2002, MNRAS, submitted (astro-ph/0201544)
Prunet S., Blanchard A., 1999, A&A, submitted (astro-ph/9909145)
Quilis V., Bower R.G., Balogh M.L., 2001, MNRAS, 328, 1091
Raymond J.C., Smith B.W., 1977, ApJS, 35, 419
Reiprich T.H., Böhringer H., 2002, ApJ, 567, 716
Renzini A., 1997, ApJ, 488, 35
Salpeter E.E., 1955, ApJ, 121, 161
Seljak U., 2002, MNRAS, submitted (astro-ph/0111362)
Somerville R.S., Primack J.R., 1999, MNRAS, 310, 1087
Springel V., White S.D.M., Tormen G., Kauffmann G., 2001, MNRAS, 328, 726
Stadel J., 2001, PhD thesis
Stanford S.A., Holden B.P., Rosati P., Eisenhardt P.R., Stern D., Squires G., Spinrad H., 2002, ApJ, 123, 619
Steinmetz M., White S.D.M., 1997, MNRAS, 288, 545
Suginohara T., Ostriker J.P., 1998, ApJ, 507, 16
Thomas P.A., Muanwong O., Kay S.T., Liddle A.R., 2002, MNRAS, 330, L48
Tozzi P., Norman C., 2001, ApJ, 546, 63 (TN01)
Treu T., Koopmans L., 2002, ApJ, submitted (astro-ph/0202342)
Valageas P., Silk J., 1999, A&A, 350, 725
Valdarnini R., 2002, ApJ, 567, 741
Viana P.T.P., Nichol R.C., Liddle A.R., 2002, ApJ, 569, L75
Voit G.M., Bryan G.L., 2001, Nat, 414, 425
Voit G.M., Donahue M., 1998, ApJ, 500, L111
Voit G.M., Bryan G.L., Balogh M.L., Bower R.G., 2002, ApJ, in press (astro-ph/0205240)

Wadsley J.W., Bond J.R., 1997, Computational Astrophysics: 12th Kingston Meeting on Theoretical Astrophysics. P. 332
White D.A., 2000, MNRAS, 312, 663
White S.D.M., Frenk C.S., 1991, ApJ, 379, 52
White S.D.M., Efstathiou G., Frenk C.S., 1993, MNRAS, 262, 1023
White D.A., Jones C., Forman W., 1997, MNRAS, 292, 419
Wu X.-P., Xue Y.-J., 2002, ApJ, 569, 112
Wu K.K.S., Fabian A.C., Nulsen P.E.J., 1998, MNRAS, 301, L20
Wu K.K.S., Fabian A.C., Nulsen P.E.J., 2000, MNRAS, 318, 889
Yamada M., Fujita Y., 2001, ApJ, 553, 145
Yoshida N., Springel V., White S.D.M., Tormen G., 2001, 535, L103

This paper has been typeset from a TEX/LATEX file prepared by the author.